HIGH-PRESSURE PHYSICS

Measuring magnetic field texture in correlated electron systems under extreme conditions

King Yau Yip[1]*, Kin On Ho[1]*, King Yiu Yu[1]*, Yang Chen[1], Wei Zhang[1], S. Kasahara[2], Y. Mizukami[3], T. Shibauchi[3], Y. Matsuda[2], Swee K. Goh[1,4]†, Sen Yang[1,4]†

Pressure is a clean, continuous, and systematic tuning parameter among the competing ground states in strongly correlated electron systems such as superconductivity and magnetism. However, owing to the restricted access to samples enclosed in high-pressure devices, compatible magnetic field sensors with sufficient sensitivity are rare. We used nitrogen vacancy centers in diamond as a spatially resolved vector field sensor for material research under pressure at cryogenic temperatures. Using a single crystal of $BaFe_2(As_{0.59}P_{0.41})_2$ as a benchmark, we extracted the superconducting transition temperature, the local magnetic field profile in the Meissner state, and the critical fields. The method developed in this work offers a distinct tool for probing and understanding a range of quantum many-body systems.

Strongly correlated electronic systems support a wide variety of phases that are sensitive to external perturbations. For example, the superconducting transition temperature T_c is sensitive to both the interaction strength and the density of states at the Fermi level (*1*), which can in turn be tuned by changing external parameters. Moreover, superconductivity is frequently found to compete with other phases, including magnetically, structurally, and electronically ordered states [for example, (*2*–*5*)]. Therefore, the ability to subject the material system to suitable tuning parameters provides a major experimental tool for reaching new phases.

One of the most successful tuning parameters is hydrostatic pressure, which changes the electronic structure and the interaction strength without introducing additional chemical inhomogeneity to the sample. For many systems, pressure is the only way to reach certain quantum states. Pressure has played an influential role in stabilizing superconductivity by suppressing the competing phases. For example, in the heavy fermion intermetallic $CePd_2Si_2$, pressure suppresses the antiferromagnetic state and induces a superconducting phase with a T_c that peaks at ~28 kbar (*2*). In the iron-based system $BaFe_2As_2$, superconductivity can similarly be induced by means of pressure on the suppression of the spin-density wave state (*6*). More recently, a superconducting state with a remarkably high T_c of 250 to 260 K has been reported in $LaH_{10-\delta}$ at ~200 GPa (*7*, *8*). These results not only reinforce the view that pressure is a powerful tuning parameter but also call for the need to study the microscopic details of superconductivity under extremely high pressure.

To generate high pressure, the sample is enclosed in a pressure cell that is orders-of-magnitude larger than the sample itself. Moreover, to ensure a stable pressure environment, electrical accessibility to the sample volume is severely restricted. Cryogenic conditions impose further restrictions. Under these demanding experimental conditions, very few detection methods can be applied. Placing a robust dc magnetic field sensor in the immediate vicinity of the sample, in particular, is a major experimental challenge.

A negatively charged nitrogen vacancy (NV) center is a point defect in diamond with a spin-1 ground state. Owing to its spin-dependent fluorescence rate, electron spin resonance (ESR) spectrum can be measured with the optically detected magnetic resonance (ODMR) method. From these spectra, we can derive the magnetic field with sensitivity of microtesla $Hz^{-1/2}$ (*9*–*13*), as well as electric field, temperature, and mechanical strain [detailed descriptions are provided in (*20*)] (*14*–*19*). NV centers can sense both the magnitude and the direction of the field, under pressures of up to 60 GPa (*16*, *21*). Furthermore, owing to its small size, a NV center naturally provides high spatial resolution, making the microscopic study of quantum many-body features possible. With these motivations in mind, we combined the field-sensing capability of NV centers and the optical accessibility of a moissanite anvil cell to probe the local magnetic field configuration around the sample at high pressures. In this work, we demonstrate and benchmark the potential of this approach by directly probing the diamagnetism associated with superconductivity in a type II superconductor, $BaFe_2(As_{0.59}P_{0.41})_2$, under pressure.

The sample we used is a piece of single crystalline $BaFe_2(As_{1-x}P_x)_2$ with x = 0.41, which comes from the ultraclean family $BaFe_2(As_{1-x}P_x)_2$ (*22*). At x = 0.33, T_c is maximized and displays clear evidence of a quantum critical point (*23*, *24*). Hence, $BaFe_2(As_{1-x}P_x)_2$ is an ideal platform with which to explore the interplay between superconductivity and quantum criticality.

An exploded view of the interior of our pressure cell is shown in Fig. 1A, and the zoom-in view illustrates the relationship between the sample and NV center reference frames. A photograph and fluorescence image in the immediate vicinity of the sample are shown in Fig. 1B. The close proximity of the microcoil to the sample ensures the efficient transmission of the microwave power to the sample space, where the NV centers are located. The bright spots in the fluorescence image are from NV centers in diamond particles, which are spread on the sample surface and mixed with pressure-transmitting fluid. The typical size of diamond particles (1 μm) was chosen to be smaller than the optical resolution for better sensitivity but larger than the vortex lattice constant a_V (*20*). In this work, three diamond particles were chosen strategically: NV_C is near the center of the sample, NV_E is off to the side near the edge of the sample, and NV_F is far away from the sample.

Under a weak external magnetic field, for $T > T_c$, the sample is in the normal state, and the magnetic field felt by the NV centers is the same as the external magnetic field (Fig. 1C). However, upon cooling below T_c, the expulsion of the magnetic field from the sample alters the field profile near the surface of the material, and this can be felt by the NV centers on the sample surface: For NV_C, the effective magnetic field is greatly reduced, whereas for NV_E, the effective magnetic field is greatly enhanced (Fig. 1D). When the superconductor is warmed across T_c, the diamagnetic response associated with superconductivity disappears at T_c. Additionally, for a type II superconductor, when the applied field is higher than the lower critical field (H_{c1}), the field begins to thread through the sample, resulting in a vortex state. The vortex state can be completely destroyed above the upper critical field (H_{c2}), at which the superconductor returns to the normal state. All these in-field behaviors can be profiled by the NV centers located right on the sample surface.

The pulse sequence shown in Fig. 2A is used to collect our ODMR data. Because the data were collected upon warming up in a weak magnetic field, our experiment probes the diamagnetism associated with superconductivity. To avoid heating caused by microwaves and laser irradiation, we devised a measurement protocol to mitigate measurement-induced

[1]Department of Physics, The Chinese University of Hong Kong, Shatin, New Territories, Hong Kong, China. [2]Department of Physics, Kyoto University, Kyoto 606-8502, Japan. [3]Department of Advanced Materials Science, University of Tokyo, Kashiwa 277-8561, Japan. [4]Shenzhen Research Institute, The Chinese University of Hong Kong, Shatin, New Territories, Hong Kong, China.
*These authors contributed equally to this work.
†Corresponding author. Email: skgoh@cuhk.edu.hk (S.K.G.); syang@cuhk.edu.hk (S.Y.)

perturbations to the superconducting state (*20*). Representative ODMR spectra at 8.3 kbar from the three diamond particles are shown in Fig. 2, B to D, when the sample temperature (~7.7 K) was much lower than T_c (~20.4 K at 8.3 kbar, determined by using ac susceptibility at zero field) (*20*). The ODMR spectra show different splittings. The splittings are caused by the Zeeman effect because of the magnetic field of the surroundings. Therefore, the ODMR spectra provides a means to detect the magnetic field. Zeeman splitting of NV_C (~64 MHz) is 10 times smaller than that of NV_E (~658 MHz) when $T < T_c$, whereas the difference is much smaller when $T > T_c$ (Fig. 2G). The ODMR spectra of NV_C at different temperatures are shown in Fig. 2E, from which the splitting was extracted and plotted in Fig. 2F. Upon warming up, the degree of splitting remains nearly constant initially but then experiences a marked increase that sets in at ~17 K. Above 21 K, the splitting levels off again. To demonstrate the relevance of this feature to superconductivity, we additionally collected the ac susceptibility data in the same experiment, which we could do because of the additional modulation coil added to our experimental configuration. Using the microcoil as the pickup coil, a sharp drop in the ac susceptibility, signifying the superconducting transition (*25*, *26*), was detected at the same temperature (Fig. 2F). The two methods agreed well on the measurement of T_c.

The change of the local magnetic field distribution can also be seen in the temperature evolution of the splitting for NV_E and NV_F (Fig. 2G). Contrary to the behavior of NV_C, the degree of splitting decreases for NV_E upon warming up. As a reference, the splitting for NV_F is nearly constant in temperature, which can be understood because NV_F is so far from the superconductor that the total field does not change. These observations are well in line with the expectation from the diamagnetism associated with superconductivity, as explained earlier. There was no noticeable change of linewidth or in the overall contrast of the ESR lines. This is because the diamond particles were much smaller in size compared with the magnetic field gradient induced by the diamagnetism associated with superconductivity. Because of the finite size of the sample and the spacing between the diamond particles and the sample, there was a residual magnetic field that caused a Zeeman splitting of ~64 MHz for NV_C at low temperatures. There was also a difference in the Zeeman splitting for three diamond particles when the sample was in the normal state because these diamond particles were randomly oriented relative to the applied magnetic field.

One of the major advantages of our technique is demonstrated in Fig. 2H. As discussed above, both the transverse and longitudinal components of the field relative to a given NV center can be calculated from its ODMR spectrum. This provides the means to reconstruct the field vector. When the sample is in the normal state, the orientation of the NV center can be calibrated against the applied field direction, which is directed along the *c* axis of the sample. This gives an effective magnetic field vector along the *c* axis that can be tracked as a function of temperature (*20*). With these considerations, we determined the effective magnetic field vector felt by NV_C, NV_E, and NV_F at 8.3 kbar. For NV_C, the field vector shortens and tilts away from the vertical direction upon entering the superconducting state. This is consistent with NV_C being on the top of the sample, and that the diamagnetism associated with superconductivity causes the field lines to bend around the sample. However, for NV_E, the field vector lengthens and only tilts slightly in the superconducting state. Again, this is consistent with NV_E being located off to the side of the sample, so that the field lines there remain vertical but denser in the Meissner state. Last, the field vector sensed by NV_F remains practically constant across the superconducting phase transition, in stark contrast to the behavior of NV_E and NV_C. The ability to collect the complete vectorial information with spatial resolution under extreme conditions

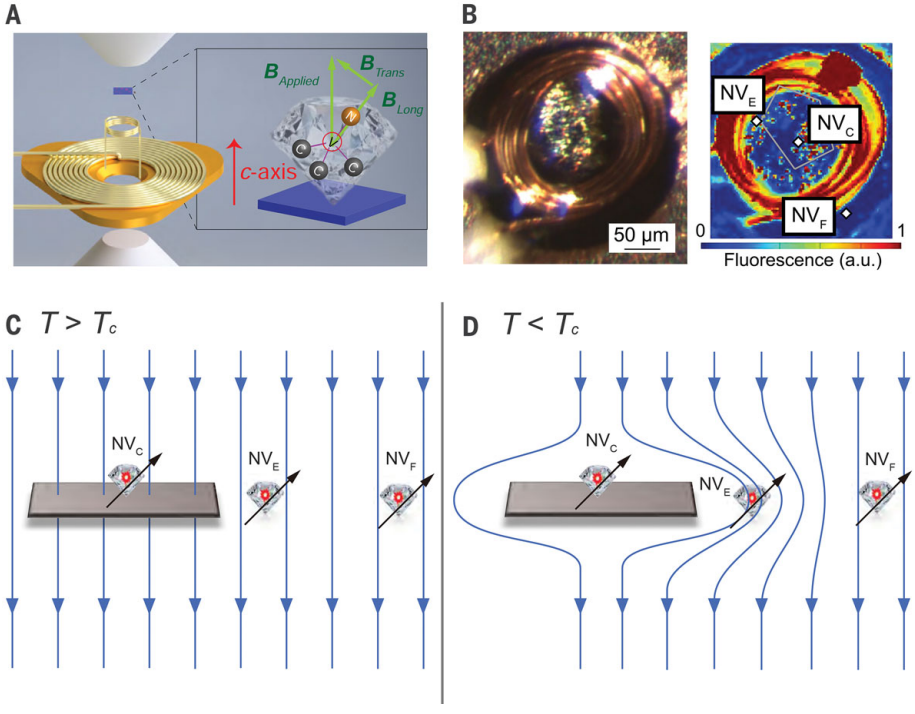

Fig. 1. Schematic illustration of experimental configurations and detection concepts. (**A**) An exploded view of our pressure cell design. The sample (blue) is located in the high-pressure chamber together with a collection of diamond particles. Each diamond particle is a sensitive local field sensor. The laser is directed toward the high-pressure chamber through the top moissanite anvil. The microwave is provided by a miniature microcoil in close proximity to the sample, allowing an efficient transmission of microwave power without causing the sample to heat up. The larger coil is added to serve as the modulation coil for auxiliary ac susceptibility measurements (*26*, *34*). The metal part beneath the modulation coil is the gasket. The zoomed-in picture shows two coordinate systems used in this study. One is the sample frame where the *c* axis is the stacking direction of the FeAs planes, and the other is the NV center frame. The external applied magnetic field in this study is always along the sample *c* axis. The diamond particles, each of which contain ~1 million NV centers with four possible quantization axes, are randomly oriented relative to the sample frame (*20*). (**B**) (Left) Photograph of the microcoil with sample on top of the anvil. (Right) Fluorescence image from the confocal scan showing the microcoil and NV centers. The shape of the sample is traced by the pentagon. The location of three particular diamond particles—NV_C, NV_E, and NV_F—are marked. NV_C is near the center of the top surface, NV_E is near the edge, and NV_F is far away from sample and serves as a control sensor. The fluorescence is collected between 650 and 800 nm. (**C** and **D**) Magnetic field profile around the sample under a weak applied magnetic field when (C) $T > T_c$ and (D) $T < T_c$. The expulsion of the magnetic field when $T < T_c$ is a consequence of the diamagnetism associated with superconductivity. The alteration of the field profile in the presence of the superconductor provides an ideal platform with which to demonstrate the performance of our sensor to probe the complete field vectors with spatial resolution under pressure.

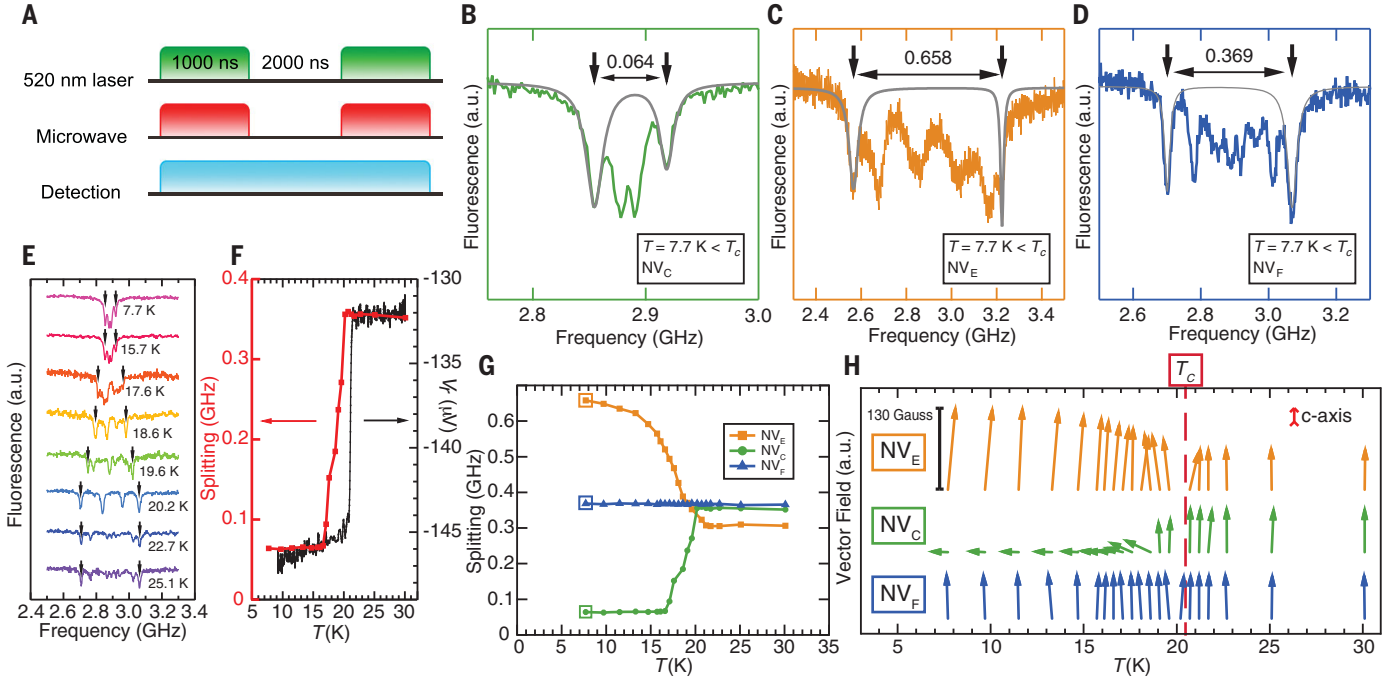

Fig. 2. The diamagnetism associated with superconductivity sensed by NV centers for $BaFe_2(As_{0.59}P_{0.41})_2$ at 8.3 kbar. (**A**) Pulse sequence used for ODMR measurements. (**B** to **D**) ODMR spectra of each diamond particle at 7.7 K. The Lorentzian fits for determining the Zeeman splitting are marked with gray lines. (**E**) ODMR spectra of NV centers in NV_C at different temperatures. (**F**) Comparison between the ODMR method (red) and ac susceptibility method (black) in determining the transition temperature T_c. (**G**) The change of the Zeeman splitting for NV centers in NV_C, NV_E, and NV_F as a function of temperature. (**H**) The variation of the local magnetic field vectors felt by NV centers in NV_C, NV_E, and NV_F across the superconducting phase transition. The vertical direction is the *c* axis of the sample. The ODMR measurements were conducted with a laser power of 10 μW and a peak microwave power of 30 mW. An external *B* field of 68 G is applied along the *c* axis of the sample.

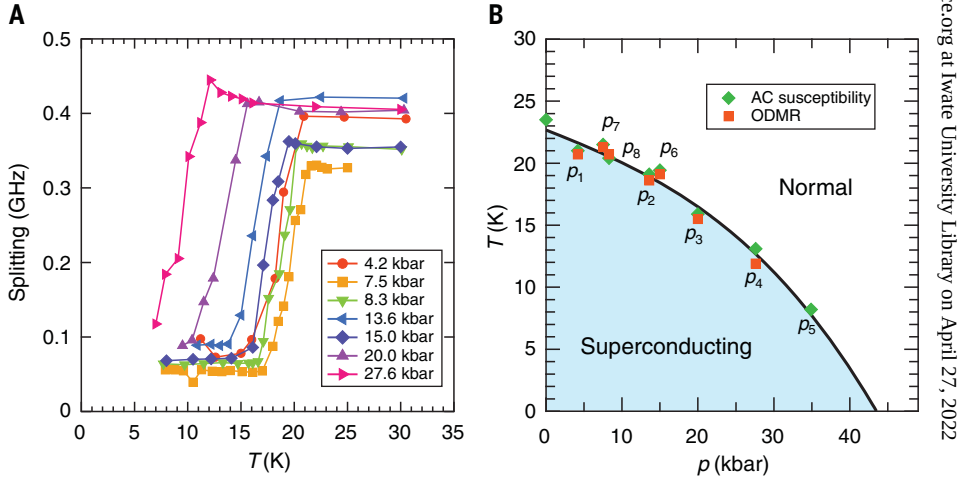

Fig. 3. Temperature-pressure phase diagram constructed for $BaFe_2(As_{0.59}P_{0.41})_2$ using NV centers. (**A**) The diamagnetism associated with superconductivity measured by the Zeeman splittings of NV centers under different pressures. The applied magnetic field is (70 ± 5) G. (**B**) The change of T_c, measured with the ODMR method (green diamond) and ac susceptibility (red square), against the applied pressure. "p_1... p_8" shows the sequence of the applied pressures. The error bars are smaller than the symbol sizes.

represents one of the key advances of our technique.

Next, we illustrate the performance of our setup under a varying pressure. In a separate run, we calibrated our ODMR shift against the shift of the ruby fluorescence spectrum up to 60 kbar, confirming our capability to sense the pressure (*20*) and to conduct ODMR experiments at high pressures. We aimed to show that our setup does not lose sensitivity to the superconducting transition when pressure is varied. The temperature dependence of the Zeeman splitting of NV_C at seven different pressure points is shown in Fig. 3A, from which the pressure dependence of T_c can be detected. Additional supporting ac susceptibility data can be found in (*20*). The resultant *T-p* phase diagram (Fig. 3B), where *p* is pressure, shows a suppression of the superconducting state with pressure. This is consistent with $x = 0.41$ being located at the overdoped side of the superconducting dome (*25*). To verify reproducibility, we also collected data on releasing pressure. The overall smooth evolution of T_c against *p* shows that the system is in the elastic regime. This series of experiments confirms the performance of our technique.

The transition width for the two methods in Fig. 2F exhibits a noticeable difference.

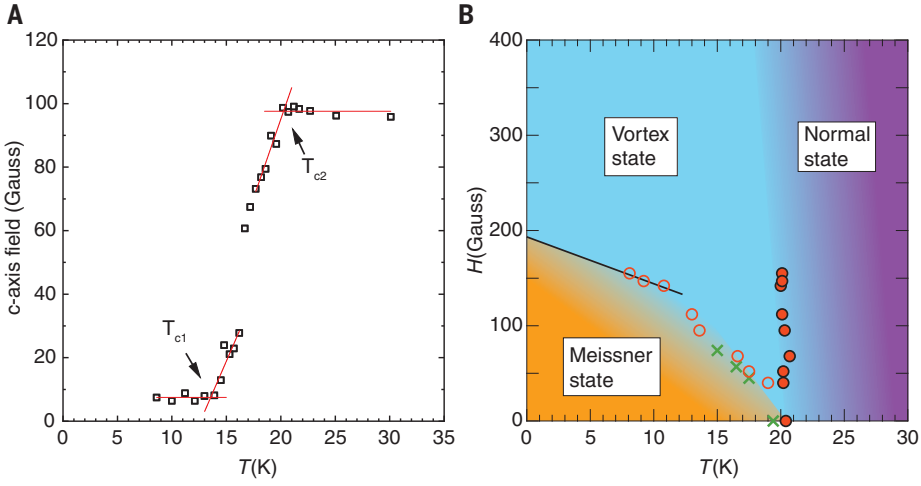

Fig. 4. Measurement of the lower critical field $H_{c1}(T)$ and the upper critical field $H_{c2}(T)$ of $BaFe_2(As_{0.59}P_{0.41})_2$. (**A**) The magnetic field along the *c* axis measured for NV_C. The applied field along the *c* axis is 95 G, which can be determined from the data at 30 K. The definitions of T_{c1} and T_{c2} are shown. (**B**) Phase diagram showing $\alpha H_{c1}(T)$ (red open circles) and $H_{c2}(T)$ (red solid circles) at 8.3 kbar. Here, the geometry factor α for a thin slab with lengths l_c along the field and l_a perpendicular to the field can be calculated by $\alpha = \tanh\sqrt{0.36(l_c/l_a)}$ (*35*), where l_c/l_a ~ 0.8. Therefore, α is ~0.5. The black line acts as a guide for the eyes. Additional $\alpha H_{c1}(T)$ for 15 kbar are added to the phase diagram for comparison (green crosses). The error bars are smaller than the symbol sizes.

This is because with the application of a magnetic field, the vortex state can be stabilized in a type II superconductor. The larger width for the ODMR-based technique is caused by the NV center, located in the close proximity of the sample, beginning to sense the penetrating field in the form of vortices (ac susceptibility, which probes the average response of the whole sample, is much less sensitive to the vortex state). To probe the phase boundaries, we calculated the magnetic field along the sample *c* axis sensed by NV_C. The temperature dependence of the resultant field at 8.3 kbar is shown in Fig. 4A. Below T_{c1} and above T_{c2}, the *c* axis field is temperature independent. However, between T_{c1} and T_{c2}, a rapid rise of the *c* axis field is detected. This is a consequence of the entry of the magnetic field lines in the form of vortices at $T > T_{c1}$ and the full penetration of the applied magnetic field for $T > T_{c2}$. Using the data at 30 K, which is in the normal state, we can calibrate the value of the applied magnetic field. Thus, this magnetic field must be proportional to H_{c1} at T_{c1} and equal to H_{c2} at T_{c2}. Hence, our ODMR data offer the possibility to detect the transition from the Meissner state to the vortex state under pressure.

Repeating the measurements at different applied fields, we can trace out $\alpha H_{c1}(T)$ and $H_{c2}(T)$ for $x = 0.41$ at 8.3 kbar (Fig. 4B), where $H_{c1}(T)$ is the boundary between the Meissner state and the vortex state, whereas $\alpha \sim 0.5$ is a numerical constant that depends on the geometry of the sample. From $H_{c1}(T)$, the temperature dependence of the London penetration depth can be deduced, allowing discussion of the superconducting gap function (*27*, *28*). $H_{c1}(T)$ appears linear at low temperatures and extrapolates to 384 G at 0 K. Both the linearity and the extrapolated $H_{c1}(0)$ value are in good agreement with previous H_{c1} studies conducted for this family of Fe-based superconductors by means of micro-Hall probe array (*27*). On the other hand, the initial slope $|dH_{c2}/dT|_{T_c}$ is proportional to the square of the quasiparticle effective mass relative to the free-electron mass. The almost vertical $H_{c2}(T)$ is consistent with the strongly correlated nature of the material system.

We have successfully demonstrated the use of NV centers in diamond as a vector magnetic field sensor with superior spatial resolution and field sensitivity in pressure cells under cryogenic conditions. The spatial resolution of the protocol shown here can be pushed to <100 nm (*20*). This resolution offers a distinct opportunity to sense the dynamics of magnetically related features such as magnetic domains, vortices (*29*–*32*), and skyrmions in pressure cells. As a noninvasive and contactless method, it can be used to study systems that are too small or too delicate for traditional macroscopic field sensors, such as flakes of two-dimensional materials (*33*). Furthermore, this approach is not limited to magnetic-field sensing. NV center is sensitive to other physical parameters, such as local electric fields and mechanical strain. Therefore, the method demonstrated here can be used in other applications besides magnetic field related processes and becomes a powerful tool in the study of quantum physics in strongly correlated systems under pressure.

REFERENCES AND NOTES

1. M. Tinkham, *Introduction to Superconductivity* (McGraw-Hill, ed. 2, 1996).
2. N. D. Mathur *et al.*, *Nature* **394**, 39–43 (1998).
3. S. S. Saxena *et al.*, *Nature* **406**, 587–592 (2000).
4. S. K. Goh *et al.*, *Phys. Rev. Lett.* **114**, 097002 (2015).
5. S. Hosoi *et al.*, *Proc. Natl. Acad. Sci. U.S.A.* **113**, 8139–8143 (2016).
6. J. Paglione, R. L. Greene, *Nat. Phys.* **6**, 645–658 (2010).
7. M. Somayazulu *et al.*, *Phys. Rev. Lett.* **122**, 027001 (2019).
8. A. P. Drozdov *et al.*, *Nature* **569**, 528–531 (2019).
9. F. Jelezko, J. Wrachtrup, *Phys. Status Solidi* **203**, 3207–3225 (2006) (a).
10. M. W. Doherty *et al.*, *Phys. Rep.* **528**, 1–45 (2013).
11. G. Balasubramanian *et al.*, *Nature* **455**, 648–651 (2008).
12. J. R. Maze *et al.*, *Nature* **455**, 644–647 (2008).
13. L. Rondin *et al.*, *Rep. Prog. Phys.* **77**, 056503 (2014).
14. P. Neumann *et al.*, *Nano Lett.* **13**, 2738–2742 (2013).
15. G. Kucsko *et al.*, *Nature* **500**, 54–58 (2013).
16. M. W. Doherty *et al.*, *Phys. Rev. Lett.* **112**, 047601 (2014).
17. A. Waxman *et al.*, *Phys. Rev. B Condens. Matter Mater. Phys.* **89**, 054509 (2014).
18. N. M. Nusran *et al.*, *New J. Phys.* **20**, 043010 (2018).
19. K. Joshi *et al.*, *Phys. Rev. Appl.* **11**, 014035 (2019).
20. Materials and methods are available as supplementary materials.
21. L. Steele *et al.*, *Appl. Phys. Lett.* **111**, 221903 (2017).
22. S. Kasahara *et al.*, *Phys. Rev. B Condens. Matter Mater. Phys.* **81**, 184519 (2010).
23. K. Hashimoto *et al.*, *Science* **336**, 1554–1557 (2012).
24. T. Shibauchi, A. Carrington, Y. Matsuda, *Annu. Rev. Condens. Matter Phys.* **5**, 113–135 (2014).
25. L. E. Klintberg *et al.*, *J. Phys. Soc. Jpn.* **79**, 123706 (2010).
26. K. Y. Yip *et al.*, *Phys. Rev. B* **96**, 020502 (2017).
27. C. Putzke *et al.*, *Nat. Commun.* **5**, 5679 (2014).
28. Y. Lamhot *et al.*, *Phys. Rev. B Condens. Matter Mater. Phys.* **91**, 060504 (2015).
29. L. Rondin *et al.*, *Nat. Commun.* **4**, 2279 (2013).
30. M. Pelliccione *et al.*, *Nat. Nanotechnol.* **11**, 700–705 (2016).
31. L. Thiel *et al.*, *Nat. Nanotechnol.* **11**, 677–681 (2016).
32. Y. Schlussel *et al.*, *Phys. Rev. Appl.* **10**, 034032 (2018).
33. Y. Cao *et al.*, *Nature* **556**, 43–50 (2018).
34. P. L. Alireza, S. R. Julian, *Rev. Sci. Instrum.* **74**, 4728–4731 (2003).
35. E. H. Brandt, *Phys. Rev. B Condens. Matter Mater. Phys.* **60**, 11939–11942 (1999).
36. K. Y. Yip *et al.*, Data for Measuring magnetic field texture in correlated electron systems under extreme conditions. Zenodo (2019); doi:10.5281/zenodo.3490189

ACKNOWLEDGMENTS

We thank D. Dasari, R. Liu, E. Shipton, J. Wrachtrup, and K. Xia for fruitful discussions. We thank S. K. Li for the technical help. **Funding:** S.K., Y.Ma., T.S., and Y.Mi. acknowledge financial supports from JST CREST (JPMJCR19T5), Grants-in-Aid for Scientific Research (KAKENHI) (15H02106, 15H03688, 15KK0160, 18H01177, 18H05227, 18K13492, 18K18727, and 19H00649) and on Innovative Areas "Topological Material Science" (15H05852) "Quantum Liquid Crystals" (19H05824) from the Japan Society for the Promotion of Science (JSPS). T.S. acknowledges the support from the Mitsubishi Foundation. S.K.G. acknowledges financial support from Hong Kong RGC (GRF/14300418, GRF/14300419, and GRF/14301316). S.Y. acknowledges financial support from Hong Kong RGC (ECS/24304617, GRF/14304618, and GRF/14304419), CUHK start-up grant, and the Direct Grants. **Author contributions:** S.K.G. and S.Y. conceived the idea, designed the experiment,

and supervised the project; S.K., Y.Ma., T.S., and Y.Mi. provided the superconductor sample; K.Y.Yip, K.O.H., K.Y.Yu, Y.C., and W.Z. prepared the pressure cell; K.Y.Yip, K.O.H., K.Y.Yu, and S.Y. performed the experiment and analyzed data; S.K.G. and S.Y. wrote the paper; and all authors commented on the manuscript. **Competing interests:** The authors declare no competing financial interests. **Data and materials availability:** All experimental data shown in the main text and supplementary materials are available at Zenodo (*36*).

SUPPLEMENTARY MATERIALS

science.sciencemag.org/content/366/6471/1355/suppl/DC1
Materials and Methods
Supplementary Text
Figs. S1 to S19
Tables S1 and S2
References (*37*–*43*)

19 December 2018; accepted 6 November 2019
10.1126/science.aaw4278

Science

Measuring magnetic field texture in correlated electron systems under extreme conditions

King Yau YipKin On HoKing Yiu YuYang ChenWei ZhangS. KasaharaY. MizukamiT. ShibauchiY. MatsudaSwee K. GohSen Yang

Science, 366 (6471), • DOI: 10.1126/science.aaw4278

Diamond-based sensors

Material properties can change dramatically under pressure. Typically, to achieve high-pressure conditions, researchers place their samples in diamond anvil cells (DACs). However, monitoring the properties of the sample inside a DAC is tricky (see the Perspective by Hamlin and Zhou). Hsieh *et al.*, Lesik *et al.*, and Yip *et al.* developed monitoring techniques based on nitrogen-vacancy (NV) centers in diamond. The NV centers can act as sensors because their energy levels and the associated spectra are sensitive to strain and magnetic fields. This enabled optical readout of a spatially resolved signal.

Science, this issue p. 1349, p. 1359, p. 1355; see also p. 1312

Science (ISSN 1095-9203) is published by the American Association for the Advancement of Science. 1200 New York Avenue NW, Washington, DC 20005. The title *Science* is a registered trademark of AAAS.